Volume 17
Number 13
1 April 2026
Pages 6245–6788

# Chemical Science

rsc.li/chemical-science

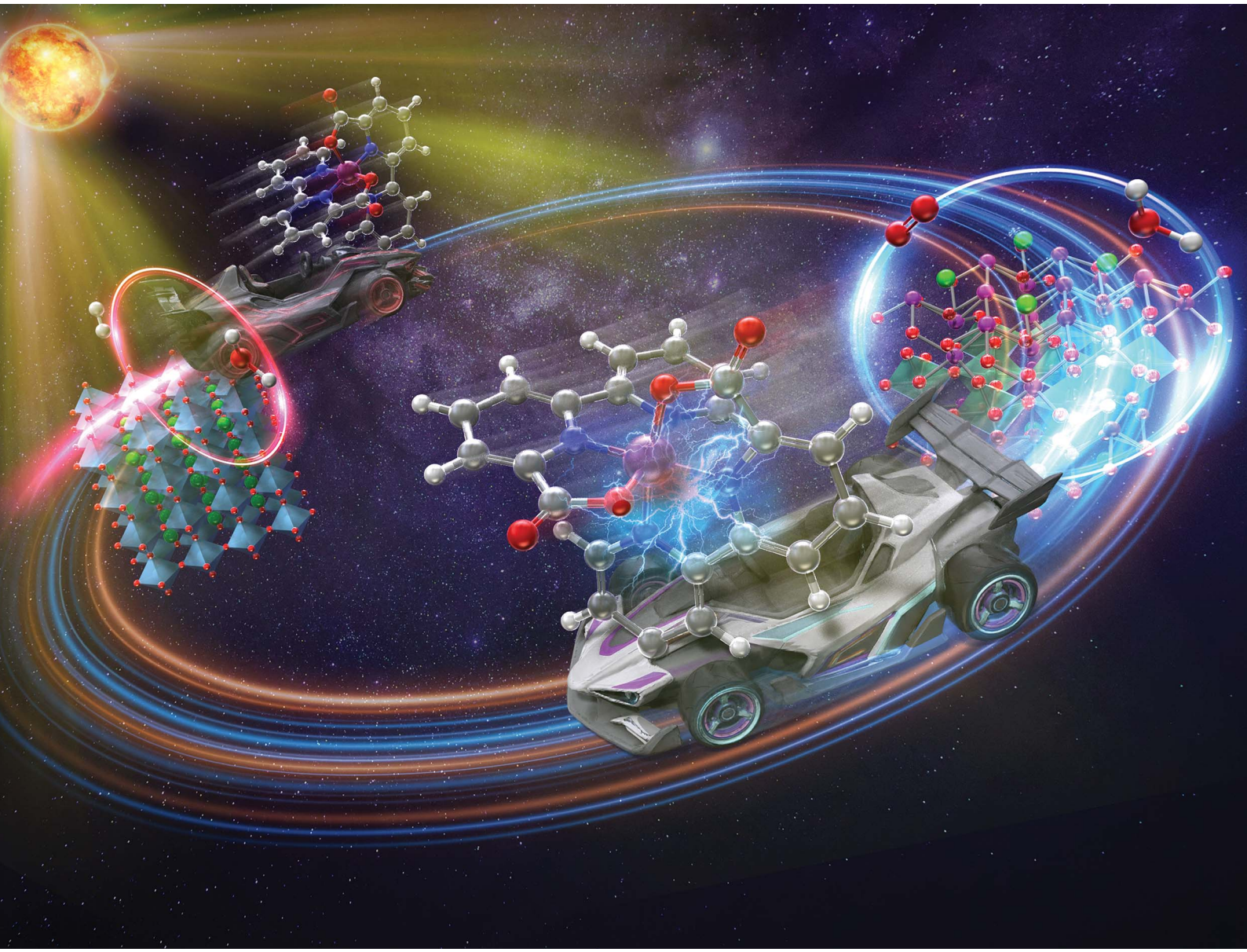

ISSN 2041-6539

**EDGE ARTICLE**

Akinobu Nakada, Ryu Abe *et al.*

Active control of forward/backward charge transfer in Z-scheme water splitting: manipulating electrostatic affinity/repulsion between photocatalyst surface and electron mediator

ROYAL SOCIETY OF CHEMISTRY

Chemical Science

ROYAL SOCIETY OF CHEMISTRY

EDGE ARTICLE

View Article Online
View Journal | View Issue



Cite this: *Chem. Sci.*, 2026, **17**, 6379

All publication charges for this article have been paid for by the Royal Society of Chemistry

# Active control of forward/backward charge transfer in Z-scheme water splitting: manipulating electrostatic affinity/repulsion between photocatalyst surface and electron mediator

Ren Itagaki,[a] Akinobu Nakada, *[a] Hajime Suzuki, [ab] Osamu Tomita [a] and Ryu Abe *[a]

Received 22nd December 2025
Accepted 14th February 2026

DOI: 10.1039/d5sc10049f

rsc.li/chemical-science

Z-scheme water splitting using semiconductor photocatalysts is a promising strategy for achieving sustainable solar hydrogen production. However, in Z-scheme systems, competition for backward electron transfer, which exerts a substantial influence on the overall quantum efficiency, is thermodynamically unavoidable. In this study, a rational strategy is proposed to overcome the backward electron transfer in Z-scheme water-splitting systems by manipulating the electrostatic affinity/repulsion between photocatalyst surfaces and electron mediators. A designed cationic/neutral charge-switchable $[Co(bpc)_2]^{+/0}$ complex selectively suppressed the backward electron transfer caused by the electrostatic repulsion between the oxidised $[Co(bpc)_2]^{+}$ form and positively surface-charged $H_2$-evolving photocatalyst, to which the forward electron transfer from the reduced $[Co(bpc)_2]^{0}$ form should be negligibly influenced by electrostatic interactions. This selective suppression of backward electron transfer enabled by charge-switchable $[Co(bpc)_2]^{+/0}$ is unique and could not be achieved using conventional cationic (*e.g.* $Fe^{3+/2+}$) or anionic (*e.g.* $IO_3^-/I^-$) redox mediators. As a result, the $[Co(bpc)_2]^{+/0}$ complex mediator provided the best photocatalytic performance for a benchmark $H_2$-evolving $SrTiO_3$:Rh photocatalyst among the conventional redox mediators and yielded a much improved apparent quantum efficiency of 2.7% for overall water splitting using $SrTiO_3$:Rh and $Bi_4TaO_8Cl$ photocatalysts. This study establishes a molecular design principle for redox mediators to improve Z-scheme water splitting, shifting the focus beyond the conventional emphasis on engineered photocatalyst materials.



## Introduction

Solar-driven water splitting using semiconductor photocatalysts has been extensively studied as a promising technology for the sustainable production of hydrogen—a clean and renewable energy carrier.[1–5] To achieve the practical production of solar hydrogen, it is imperative to efficiently utilise the visible light region, as this accounts for almost half of the solar energy that reaches the Earth's surface.[6] Numerous efforts have been made to develop visible light-responsive semiconductor materials as photocatalysts.[7] However, only a limited number of studies have reported successful overall water splitting by employing a single photocatalyst material.

To overcome this limitation, considerable attention has been directed toward Z-scheme water-splitting systems inspired by natural photosynthesis.[7,8] In a typical Z-scheme configuration, two distinct semiconductor photocatalysts, one responsible for $H_2$ evolution and the other responsible for $O_2$ evolution, are interconnected *via* a reversible electron mediator (redox couple) in solution. To date, various semiconductor photocatalysts, which could not solely split water, have been applied to Z-scheme water splitting because each photocatalyst only needs to drive $H_2$ or $O_2$ evolution with the redox species in the Z-scheme system.

However, in addition to the aforementioned benefits, the Z-scheme system has an inherent drawback, that is, competitive backward electron transfer reactions.[8] The electron mediator must have reversible redox properties with a redox potential between the conduction band minimum (CBM) of the $O_2$-evolving photocatalyst (OEP) and the valence band maximum (VBM) of the $H_2$-evolving photocatalyst (HEP), as shown in Fig. 1a. Although an appropriate redox potential enables electron transportation from photoexcited OEP to HEP (red arrows in Fig. 1a), electron transfer in the backward direction, *i.e.*, from HEP to OEP (blue arrows in Fig. 1a), is possible. In Z-scheme systems, competition for backward electron transfer, which exerts a substantial influence on the overall quantum efficiency, is thermodynamically unavoidable. Therefore, a substantial body of research has been dedicated to mitigating backward

[a]*Department of Energy and Hydrocarbon Chemistry, Graduate School of Engineering, Kyoto University, Nishikyo-ku, Kyoto 615-8510, Japan. E-mail: nakada@scl.kyoto-u.ac.jp; ryu-abe@scl.kyoto-u.ac.jp*

[b]*Precursory Research for Embryonic Science and Technology (PRESTO), Japan Science and Technology Agency (JST), 4-1-8 Honcho, Kawaguchi, Saitama 332-0012, Japan*

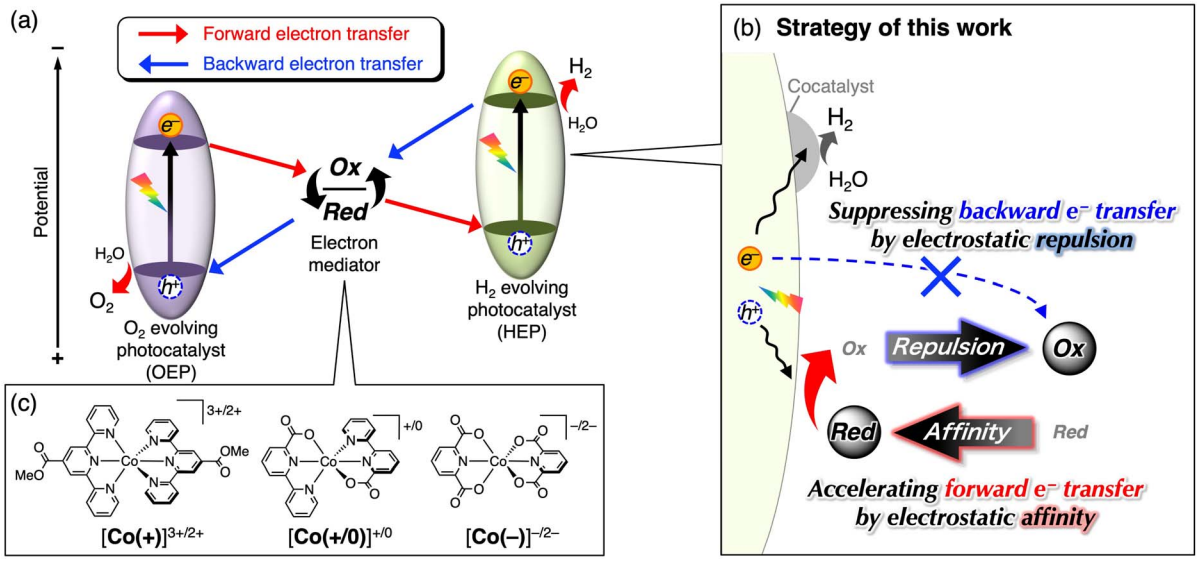


Fig. 1 (a) Schematic of Z-scheme electron transportation and backward electron transfer, (b) strategy of this work to suppress backward electron transfer: controlling electrostatic interaction by modulating charges of the photocatalyst surface and electron mediator, and (c) molecular structures and abbreviations of cobalt complexes as an electron mediator used in this study.

electron transfer, and most studies have focused on surface modifications, including cocatalyst loading.[9–13]

Regarding the electron mediator species, some redox compounds, such as $IO_3^-/I^-$, $Fe^{3+/2+}$, $[Fe(CN)_6]^{3-/4-}$, $[Co(bpy)_3]^{3+/2+}$, and polyoxometalates (POMs), have been applied to Z-scheme water splitting.[14–18] The selection of electron mediators for combination with semiconductor photocatalysts has mainly been based on their redox potentials and stability at the pH of the reaction solution. However, clear guidelines for electron mediator selection with respect to resistance toward backward electron transfer are lacking, and thus choices have largely relied on "invisible" empirical compatibility in the specific combination of mediator and photocatalyst material.

In this study, a rational strategy to address the persistent challenge of backward electron transfer was developed with specific focus on the electrostatic affinity and repulsion between the photocatalyst surface and electron mediators (Fig. 1b). Three cobalt complexes with different charges were prepared: cationic $[Co(tpyCO_2Me)_2]^{3+/2+}$ (**Co(+)**), anionic $[Co(dipic)_2]^{-/2-}$ (**Co(−)**), and cationic/neutral $[Co(bpc)_2]^{+/0}$ (**Co(+/0)**) (Fig. 1c). Because inorganic semiconductor particles have specific surface charges that can be tuned by changing the solution pH,[19] the effects of various combinations of mediator/surface charges on forward and backward electron transfer were systematically investigated. In particular, we aimed to actively control the electrostatic affinity/repulsion caused by photoinduced electron transfer to suppress backward electron transfer using the neutral-to-cationic charge-switching nature of a novel $[Co(bpc)_2]^{+/0}$ complex.

## Results and discussion

### Properties of cobalt complexes as a redox mediator

The homoleptic $Co^{II}$ complexes (Fig. 1c) with tridentate ligands—methyl 2,2′:6′,2″-terpyridine-4′-carboxylate ($tpyCO_2Me$), 2,2′-bipyridine-6-carboxylate ($bpc^-$), or dipicolinate ($dipic^{2-}$)—were synthesised by mixing $CoCl_2 \cdot 6H_2O$ with the corresponding ligand (2 eq.) in methanol, as well as tetramethylammonium hydroxide in the case for carboxylate ligands. The corresponding oxidised forms ($Co^{III}$) were prepared by reacting the $Co^{II}$ complexes with a nitrosonium ion ($NO^+$). The Co complexes showed negligible absorption in the visible region ($\lambda > 400$ nm), except for **[Co(+)]**$^{2+}$, which showed weak absorption attributed to metal-to-ligand charge transfer arising from the lower $\pi^*$ level of $tpyCO_2Me$ (Fig. S1).[20] Even for **[Co(+)]**$^{2+}$, the molar extinction coefficient was not large ($\sim$2000 $M^{-1}$ $cm^{-1}$). Therefore, the inner filter effect (shielding of light absorption of the photocatalyst) by the Co complexes would be small.

The redox potential of an electron mediator for Z-scheme water splitting must be more positive than the conduction band minimum (CBM) of the OEP and more negative than the valence band maximum (VBM) of the HEP (Fig. 1a). The cobalt complexes **[Co(+)]**$^{2+}$, **[Co(+/0)]**$^0$, and **[Co(−)]**$^{2-}$ each exhibited a single redox wave corresponding to the metal-centred $Co^{3+/2+}$ at $E_{1/2}$ = +0.17, +0.25, and +0.53 V *vs.* Ag/AgCl, respectively (Fig. 2a). The redox peak separations ($\Delta E$) for **[Co(+)]**$^{2+}$ and **[Co(+/0)]**$^0$ were *ca.* 70 mV, which is close to ideal reversibility. In contrast, the $\Delta E$ for the **[Co(−)]**$^{-/2-}$ redox reaction is approximately as large as 780 mV, suggesting slow electron transfer kinetics and/or the existence of protonation/deprotonation processes. However, the redox reaction was repeatable including **[Co(−)]**$^{-/2-}$ (Fig. S2), and the $E_{1/2}$ value was constant over a range of pH values for all three Co complexes (Fig. 2b). Importantly, all $Co^{III}$ complexes are suitable as redox mediators because their $E_{1/2}$ values are between the CBM of representative OEP (*e.g.*, $WO_3$,[13] $BiVO_4$,[21] and $Bi_4TaO_8Cl$[22]) and the VBM of HEP (*e.g.*, $SrTiO_3$:Rh[23] and TaON[24]), as summarised in Fig. 2b and c.

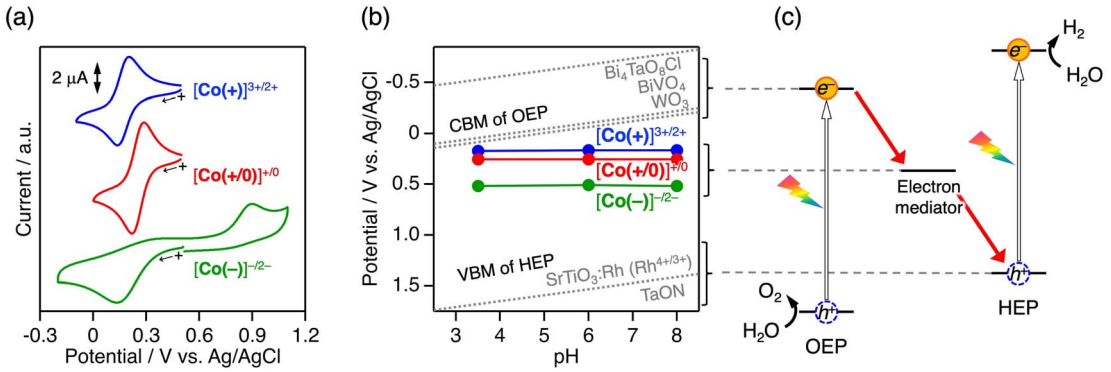


Fig. 2 (a) Cyclic voltammograms of the cobalt complexes (0.3 mM) in aqueous NaCl (0.1 M) solution at pH 3.5 (adjusted with HCl) and (b) potentials of cobalt complexes as the redox mediator, CBM of OEP ($WO_3$, $BiVO_4$, and $Bi_4TaO_8Cl$), and VBM of HEP ($SrTiO_3$:Rh and TaON), in which the band potentials of semiconductor photocatalysts are assumed to follow Nernst relationship.[25–27] (c) Energy diagram of Z-scheme water splitting.

### Manipulation of electrostatic interactions on redox-mediated $H_2$ evolution

Fig. 3 shows the time course of visible-light-driven $H_2$ evolution on M/$SrTiO_3$:Rh (M = Pt or $CrO_x$/Pt) photocatalysts using three different $Co^{II}$ complexes as electron donors. Among the three $Co^{II}$ complexes, $[Co(+/0)]^0$ induced the most efficient $H_2$ evolution, although the driving force for electron transfer was similar to that of $[Co(+)]^{2+}$. The $CrO_x$ shell coating on the Pt cocatalyst (Fig. S3) further improved the $H_2$ evolution rate by 2.1 times when using $[Co(+/0)]^0$ (red lines in Fig. 3a and b). The $CrO_x$ shell coated on the Pt cocatalyst has been known to block the penetration of redox species into the Pt catalyst centre while allowing $H^+$.[9,28] Thus, the $CrO_x$ coating improved the $H_2$ evolution activity by suppressing backward electron transfer (re-reduction of the oxidised electron donor) on the cocatalyst core. The use of $[Co(-)]^{2-}$ resulted in negligible $H_2$ evolution activity over Pt/$SrTiO_3$:Rh, whereas the $CrO_x$ overlayer significantly improved the activity by 16.5 times, although it was still the lowest among the three complexes. In contrast, the $CrO_x$ coating had only a minor effect (approximately 1.2-fold enhancement) on the rate of photocatalytic activity when $[Co(+)]^{2+}$ was used.

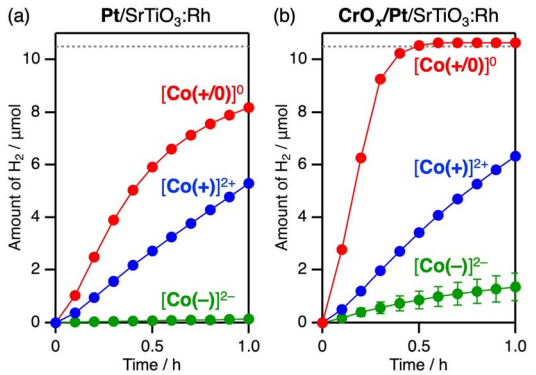


Fig. 3 Time courses of $H_2$ evolution using (a) Pt- or (b) $CrO_x$/Pt-loaded $SrTiO_3$:Rh (10 mg) in an aqueous solution (70 mL, pH 3.5) containing $[Co(+)]^{2+}$, $[Co(+/0)]^0$, or $[Co(-)]^{2-}$ (0.3 mM each) as an electron donor under visible-light irradiation ($\lambda = 430$ nm). The broken lines show the upper limit of $H_2$ evolution expected from the amount of $Co^{II}$ species added to the solutions.

Interestingly, the degree of impact of the $CrO_x$-shell coating on improving $H_2$ evolution activity differed significantly depending on the Co complex used ($[Co(-)]^{2-}$ (16.5 times) > $[Co(+/0)]^0$ (2.1 times) > $[Co(+)]^{2+}$ (1.2 times)). Electrostatic interactions between the photocatalyst surface and Co complex with different charges were considered to understand the different efficacies of the $CrO_x$ shells in suppressing backward electron transfer. Although no significant adsorption of Co complexes onto $CrO_x$/Pt/$SrTiO_3$:Rh was observed (Fig. S4), dynamic electrostatic interaction in the reaction dispersion cannot be excluded. After serving as an electron donor, the total valence states of the oxidised Co complexes $[Co(+)]^{3+}$, $[Co(+/0)]^+$, and $[Co(-)]^-$ are +3, +1, and −1, respectively. Because the surface zeta potential of M/$SrTiO_3$:Rh is positive (+43 mV) at pH 3.5, only $[Co(-)]^-$ could be electrostatically attracted to the positively charged photocatalyst surface (Fig. 4a). Therefore, $[Co(-)]^-$ would have greater opportunities for backward electron transfer, resulting in negligible $H_2$ evolution activity on Pt/$SrTiO_3$:Rh. Once the backward electron transfer on Pt was protected by the $CrO_x$ shell, $[Co(-)]^{2-}$ provided improved activity because the electrostatic affinity between $[Co(-)]^{2-}$ and the positively charged photocatalyst favours forward electron transfer. However, even if the Pt surface is protected by the $CrO_x$ shell, there are still significant opportunities for backward electron transfer on the $SrTiO_3$:Rh surface before the photoexcited electrons reach the Pt cocatalyst core (Fig. 4a). Therefore, $[Co(-)]^{2-}$ still exhibited low activity even when a $CrO_x$-shell coating was applied. In contrast, $[Co(+)]^{3+/2+}$ experiences electrostatic repulsion with the photocatalyst in both its oxidised and reduced forms. This electrostatic repulsion possibly inhibited not only the backward electron transfer but also the forward electron transfer (Fig. 4b), resulting in a negligible effect of the $CrO_x$ coating when $[Co(+)]^{2+}$ was used as the mediator. Notably, the superior performance of $[Co(+/0)]^0$ should originate from its "charge-switching" nature. Regarding the backward electron transfer, $[Co(+/0)]^+$ induces electrostatic repulsion, as in the case of $[Co(+)]^{3+}$. In contrast, neutral [Co(+/

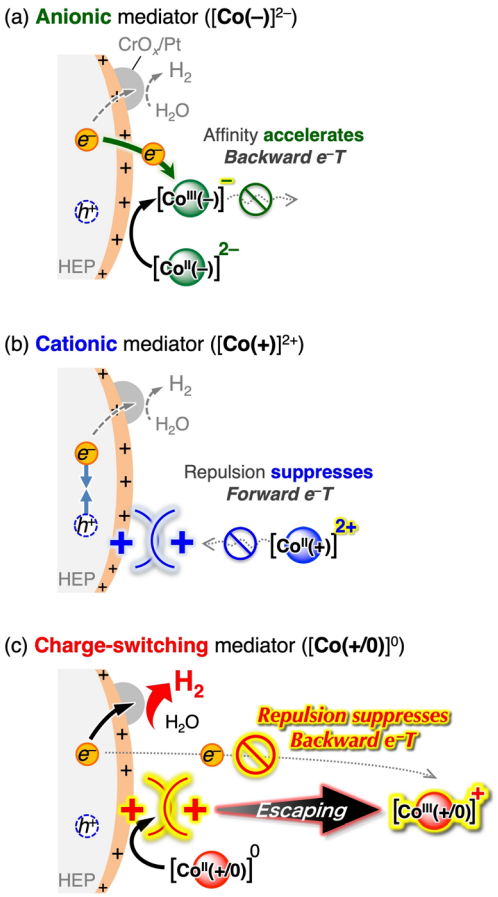


Fig. 4 Plausible schematic illustration of photoinduced electron transfer and backward electron transfer processes at pH 3.5 between $CrO_x$/Pt/$SrTiO_3$:Rh and (a) anionic, (b) cationic, and (c) charge-switching mediators.

**0**)]$^0$, which does not induce electrostatic interactions, should not inhibit the forward electron transfer, in stark contrast to the case of [**Co(+)**]$^{2+}$. Consequently, it is supposed that the "charge-switching" [**Co(+/0)**]$^0$ enables selective suppression of backward electron transfer without decelerating forward electron transfer with a positively charged photocatalyst (Fig. 4c).

The hypothesis that electrostatic interaction manipulates backward electron transfer was further investigated by adding oxidised redox mediators to $H_2$ evolution photocatalysis. Table 1 shows the rates of $H_2$ evolution over $CrO_x$/Pt/$SrTiO_3$:Rh photocatalysts with various reversible electron donors in the presence and absence of the corresponding oxidised compound. In addition to the conventional $Fe^{3+/2+}$ system,[29] the $H_2$ evolution rates obtained using $Fe^{2+}$, [**Co(+)**]$^{2+}$, or [**Co(+/0)**]$^0$ did not significantly decrease upon the addition of the corresponding cationic electron acceptor (*i.e.*, $Fe^{3+}$, [**Co(+)**]$^{3+}$, or [**Co(+/0)**]$^+$). In contrast, pronounced reductions in photocatalytic activity were observed in anionic redox systems, including $I^-$,[30] [**Co(–)**]$^{2-}$, and $[SiVW_{11}O_{40}]^{6-}$.[31] The decreased $H_2$ evolution rate can be attributed to the competition between the reducing protons and oxidised redox compounds (Fig. 4a). Based on the above overall trend, we can conclude that the positively charged surface of $CrO_x$/Pt/$SrTiO_3$:Rh (zeta potential of +43 mV) is beneficial for suppressing backward electron transfer from the positively charged redox species. Notably, [**Co(+/0)**]$^0$ provided higher $H_2$ evolution rate than cationic electron donors. [**Co(+/0)**]$^0$ and [**Co(+)**]$^{2+}$ have similar redox potentials but may have different steric effects from their ligands, which would affect the photocatalytic performance. However, introducing $[Co(tpy)_2]^{2+}$, which is a cationic complex similar to [**Co(+)**]$^{2+}$ but without methyl ester ligand, resulted in an activity similar to that of [**Co(+)**]$^{2+}$ and much lower than that of [**Co(+/0)**]$^0$. Therefore, the superior performance of [**Co(+/0)**]$^0$ as the mediator for $H_2$ evolution should originate from its "charge-switching" nature that enabled selective suppression of backward electron transfer without decelerating forward electron transfer with a positively charged photocatalyst (Fig. 4c). Therefore, [**Co(+/0)**]$^0$ most effectively exploits the intrinsic potential of $CrO_x$/Pt/$SrTiO_3$:Rh for $H_2$ evolution, outperforming various well-known conventional reversible electron donors. Under these conditions, an apparent quantum efficiency (AQE) of 5.1% at 430 nm was achieved for $H_2$ evolution using $CrO_x$/Pt/$SrTiO_3$:Rh with [**Co(+/0)**]$^0$ at pH 3.5.

Upon increasing the solution pH, the photocatalytic $H_2$ evolution activity of $CrO_x$/Pt/$SrTiO_3$:Rh with [**Co(+/0)**]$^0$ decreased (Fig. 5a). This trend could not be simply explained by the decreased $H^+$ concentration because the activity increased at high pH when MeOH was used as an irreversible sacrificial reductant (Fig. 5b). Therefore, the pH dependence should be derived based on the electron transfer process with the electron mediator.

The surface zeta potential of $CrO_x$/Pt/$SrTiO_3$:Rh decreased with increasing solution pH and flipped to negative at pH 6.0 (Fig. 6a). Importantly, the inhibitory effects caused by the addition of [**Co(+/0)**]$^+$ also largely depended on the solution pH (Fig. 6b). As discussed above, the rate of $H_2$ evolution remained almost unchanged when [**Co(+/0)**]$^+$ was added at pH 3.5 (zeta potential = +43 mV). However, the durability against backward electron transfer weakened as the pH increased to 6.0 (zeta potential = ~0) and 8.0 (zeta potential = −16 mV), where electrostatic repulsion with [**Co(+/0)**]$^+$ was not expected. Similar relationship between zeta potential and photocatalytic activity was observed when using $ZrO_2$/TaON (Fig. S5), which is another benchmark HEP.[35] Although photoexcitation can shift the zeta potential to some extent, the overall trend suggests the importance of manipulating electrostatic interaction by appropriately tuning the surface charge and the "charge-switchable" redox mediator.

In summary, the electrostatic affinity/repulsion between the redox mediators and photocatalyst surface plays an important role in forward and backward electron transfer when using reversible electron donors ($Co^{II}$ complexes) for photocatalytic $H_2$ evolution (Fig. 4 and 6). The reduced and oxidised forms of [**Co(+)**]$^{3+/2+}$ are both cationic complexes, whereas those of [**Co(–)**]$^{-/2-}$ are both anionic complexes, indicating that their charged nature (cationic or anionic) is maintained during redox events. For instance, if the photocatalyst surface charge is positive, electrostatic repulsion with cationic [**Co(+)**]$^{3+/2+}$ is unfavourable for accelerating forward electron transfer, but favourable for suppressing backward electron transfer (Fig. 4b).

Table 1 Initial rates of $H_2$ evolution over $CrO_x$/Pt/$SrTiO_3$:Rh with various electron donors and acceptors[a]

| Charge of redox species | Donor | $E_{Donor}$/V[b] | Additive | Rate of $H_2$ evolution/μmol $h^{-1}$ | Retention ratio of $H_2$ evolution rate |
|---|---|---|---|---|---|
| Cationic | $Fe^{2+}$ [c] | 0.56 (ref. 32) | — | 9.8 | 0.94 |
| | | | $Fe^{3+}$ | 9.2 | |
| | $[Co(+)]^{2+}$ | 0.17 | — | 7.7 | 0.95 |
| | | | $[Co(+)]^{3+}$ | 7.3 | |
| | $[Co(tpy)_2]^{2+}$ | 0.10 (ref. 33) | — | 5.5 | 0.98 |
| | | | $[Co(tpy)_2]^{3+}$ | 5.4 | |
| Neutral/Cationic | $[Co(+/0)]^0$ | 0.25 | — | 27.8 | 0.97 |
| | | | $[Co(+/0)]^+$ | 27.1 | |
| Anionic | $I^-$ | 0.67 (ref. 34) | — | 9.2 | 0.09 |
| | | | $IO_3^-$ | 0.8 | |
| | $[Co(-)]^{2-}$ | 0.53 | — | 2.7 | 0.44 |
| | | | $[Co(-)]^-$ | 1.2 | |
| | $[SiVW_{11}O_{40}]^{6-}$ | 0.48 (ref. 31) | — | 7.1 | 0.42 |
| | | | $[SiVW_{11}O_{40}]^{5-}$ | 3.0 | |

[a] Standard conditions: $CrO_x$/Pt/$SrTiO_3$:Rh (10 mg) in an aqueous solution (70 mL, pH 3.5) containing an electron donor (0.3 mM) in the absence or presence of the corresponding oxidised form as an additive (0.3 mM) under visible light irradiation ($\lambda = 430$ nm). [b] *vs.* Ag/AgCl. [c] Performed at pH 2.4.

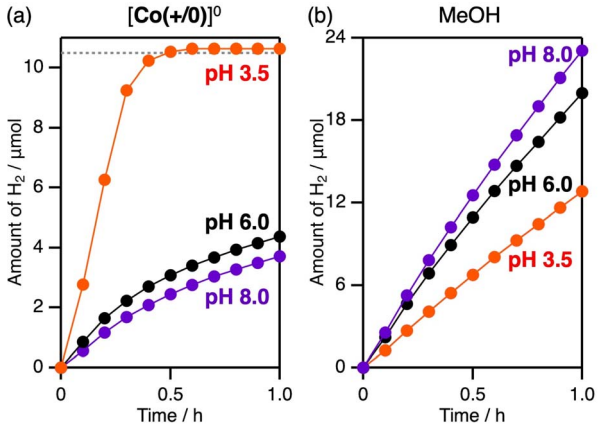


Fig. 5 Time courses of $H_2$ evolution using $CrO_x$/Pt/$SrTiO_3$:Rh (10 mg) in an aqueous solution (70 mL) containing (a) 0.3 mM $[Co(+/0)]^0$ or (b) 10 vol% MeOH as an electron donor at pH 3.5, 6.0, or 8.0 (adjusted with HCl) under visible-light irradiation ($\lambda = 430$ nm).

This situation is reversed when anionic $[Co(-)]^{-/2-}$ is used or when the photocatalyst has a negative surface charge, *i.e.*, accelerating both forward and unfavourable backward electron transfer (Fig. 4a). Therefore, when $[Co(+)]^{3+/2+}$ and $[Co(-)]^{-/2-}$ are used, enhancement of forward electron transfer inevitably occurs at the expense of increased backward electron transfer, resulting in an inherent trade-off. Notably, although many redox mediators have been employed in Z-scheme water splitting (*e.g.*, $Fe^{3+/2+}$, $IO_3^-/I^-$, $[Fe(CN)_6]^{3-/4-}$, $[Co(bpy)_3]^{3+/2+}$, and anionic polyoxometalates), all conventional redox mediators are both cationic or anionic pairs. In contrast, "charge switching" $[Co(+/0)]^{+/0}$ can cancel out the trade-off, and only the backward electron transfer with the cationic oxidised form $[Co(+/0)]^+$ is affected by the electrostatic interaction and has a chance to be suppressed when the surface charge is positive (Fig. 4c and 6c). Therefore, we can conclude that $[Co(+/0)]^0$ provides distinct $H_2$ evolution activities for positively charged $SrTiO_3$:Rh and TaON (enabled in acidic conditions).

## Z-scheme water splitting using Co complexes as a redox mediator

Prior to demonstrating Z-scheme overall water splitting, photocatalytic water oxidation was tested with the oxidised form of the three $Co^{III}$ complexes using $PtO_x/WO_3$ (ref. 36) as an OEP. Among the three $Co^{III}$ complexes, $[Co(+/0)]^+$ provided the best water oxidation activity for $PtO_x/WO_3$ (Fig. 7a), despite having a smaller thermodynamic driving force for electron transfer than $[Co(-)]^-$ (Fig. 2). Considering the electrostatic interactions, the zeta potential of $WO_3$ always remained negative (Fig. 7b), and the rate of $O_2$ evolution remained unchanged, regardless of the solution pH. Negligible pH dependency of photocatalytic $O_2$ evolution was also found using $AgNO_3$ as a sacrificial electron acceptor (Fig. S6). Hence, the backward electron transfer with $[Co(+/0)]^{+/0}$ does not seem to be influenced by the solution pH during the photocatalytic water oxidation over $WO_3$. Similar to the case of $H_2$ evolution, a trade-off between forward and backward electron transfer was considered due to electrostatic effects when cationic $[Co(+)]^{3+/2+}$ or anionic $[Co(-)]^{-/2-}$ mediators were employed. For example, $[Co(-)]^-$ induced stable water oxidation without a decrease in the $O_2$ evolution rate, although the rate was low. This is reasonable considering that the surface charge of $PtO_x/WO_3$ is negative (Fig. 7b), and both forward and backward electron transfers decelerate in the anionic $[Co(-)]^{-/2-}$ system. In the case of the charge-switchable $[Co(+/0)]^{+/0}$ system, forward electron transfer from $PtO_x/WO_3$ to $[Co(+/0)]^+$ is potentially favoured due to its electrostatic affinity, whereas the generated $[Co(+/0)]^0$ is not influenced by the electrostatic interactions. This explains the superior $O_2$ evolution activity of $[Co(+/0)]^+$ as an electron acceptor.

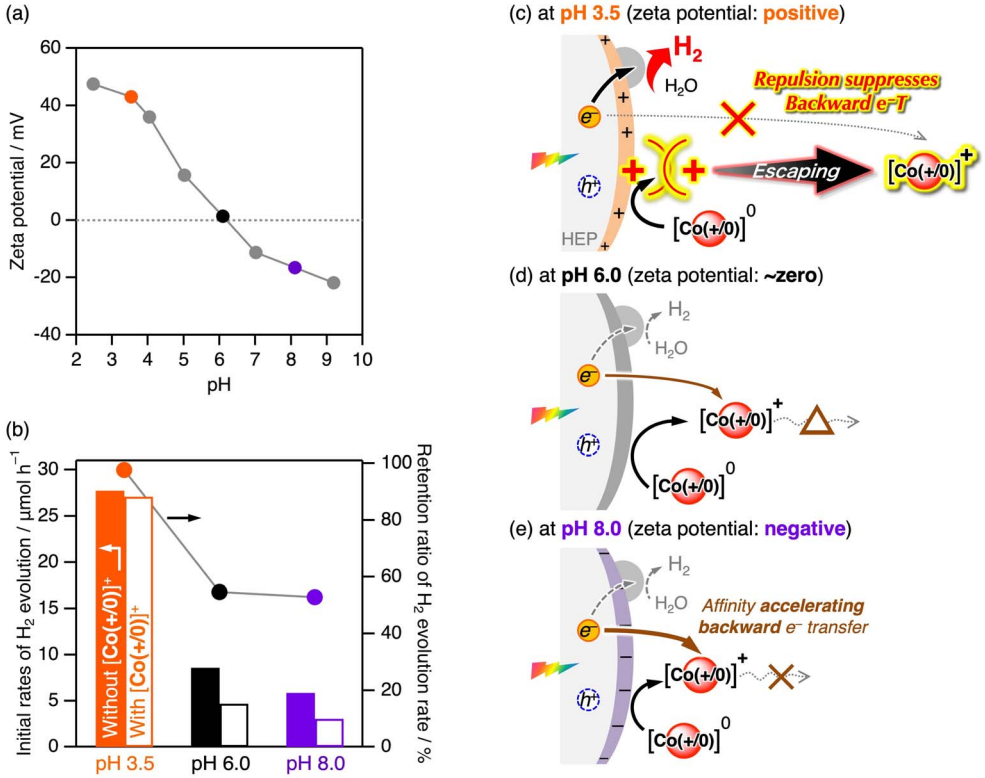


Fig. 6 (a) pH dependent zeta potentials and (b) initial rates of $H_2$ evolution using $CrO_x$/Pt/$SrTiO_3$:Rh (10 mg) in an aqueous solution containing $[Co(+/0)]^0$ (0.3 mM) as an electron donor in the absence or presence of $[Co(+/0)]^+$ (0.3 mM) at pH 3.5, 6.0, or 8.0 (adjusted with HCl) under visible-light irradiation ($\lambda = 430$ nm). The right axis shows the retention ratio of the $H_2$ evolution rate, which is the ratio of the rate in the presence of $[Co(+/0)]^+$ to the rate in its absence. Plausible schematic illustration of photoinduced electron transfer and backward electron transfer processes between $CrO_x$/Pt/$SrTiO_3$:Rh and cobalt complexes at (c) pH 3.5, (d) pH 6.0, and (e) 8.0 under different electrostatic interactions.

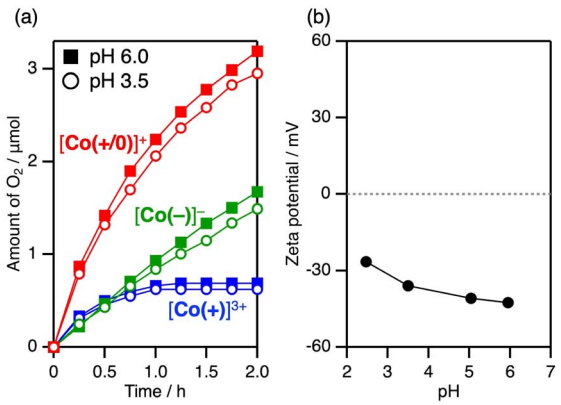


Fig. 7 (a) Time courses of $O_2$ evolution using $PtO_x/WO_3$ (35 mg) in an aqueous solution (70 mL) containing $[Co(+)]^{3+}$, $[Co(+/0)]^+$, or $[Co(-)]^-$ (0.3 mM each) as an electron acceptor at pH 3.5 or 6.0 (adjusted with HCl or NaOH) under visible-light irradiation ($\lambda = 430$ nm) and (b) pH-dependency of zeta potentials of $PtO_x/WO_3$.

When $BiVO_4$ or $Bi_4TaO_8Cl$ was applied as the OEP with the aid of a $[Co(+/0)]^+$ acceptor, the $O_2$ evolution activity was influenced by the solution pH (Fig. S7). At pH 3.5, both $BiVO_4$ and $Bi_4TaO_8Cl$ have positive charges, which leads to electrostatic repulsion with $[Co(+/0)]^+$ and was therefore unfavourable for electron transfer. Consequently, they showed decreased $O_2$ evolution activity compared to conditions where the surface charge was negative (at pH 6 for $BiVO_4$ and pH 8 for $Bi_4TaO_8Cl$; Fig. S7). The best AQE for $O_2$ evolution was 4.7% at 430 nm, achieved using (Fe,Ru)$O_x$/$Bi_4TaO_8Cl$ with $[Co(+/0)]^+$ at pH 8.0.

Overall water splitting into $H_2$ and $O_2$ proceeded in the presence of $[Co(+/0)]^{+/0}$ as a redox mediator in combination with $CrO_x$/Pt/$SrTiO_3$:Rh and $PtO_x/WO_3$ (entry 1, Table 2). On the other hand, simultaneous $H_2$ and $O_2$ generation was not observed in the absence of $CrO_x$/Pt/$SrTiO_3$:Rh, $PtO_x/WO_3$, or Co complexes (entries 2–4). Therefore, we can conclude that the Co complexes act as redox mediators in Z-scheme water splitting with $CrO_x$/Pt/$SrTiO_3$:Rh and $PtO_x/WO_3$ as $H_2$- and $O_2$-evolving photocatalysts, respectively. The overall water splitting proceeded stably for several cycles of photocatalysis tests (Fig. S8).

Among the three Co complexes, "charge switching" $[Co(+/0)]^{+/0}$ induced the best water splitting performance (entries 1, 5 and 6 in Table 2). This trend is reasonable considering their performance in half-reactions (Fig. 3b and 7a). During steady Z-scheme operation with the $[Co(+)]^{3+/2+}$ mediator, the oxidised form ($Co^{III}$; $[Co(+)]^{3+}$) was dominant in the solution (entry 5 in Table 2) because water oxidation photocatalysis was much slower than $H_2$ evolution (Fig. 3b and 7a). In contrast, for the anionic $[Co(-)]^{-/2-}$ mediator, $Co^{II}$ was dominant species under steady state conditions (entry 6 in Table 2), because the

Table 2 Rates of $H_2$ and $O_2$ evolution through Z-scheme water splitting under various conditions[a]

| Entry | HEP | OEP | Mediator | $H_2$ rate/μmol $h^{-1}$ | $O_2$ rate/μmol $h^{-1}$ | $Co^{II}$ : $Co^{III}$ |
|---|---|---|---|---|---|---|
| 1 | $CrO_x$/Pt/$SrTiO_3$:Rh | $PtO_x/WO_3$ | $[Co(+/0)]^+$ | 11.7 | 5.4 | 1 : 9 |
| 2 | — | $PtO_x/WO_3$ | $[Co(+/0)]^+$ | N.D.[b] | 4.5 | 9 : 1 |
| 3 | $CrO_x$/Pt/$SrTiO_3$:Rh | — | $[Co(+/0)]^+$ | N.D. | N.D. | 0 : 10 |
| 4 | $CrO_x$/Pt/$SrTiO_3$:Rh | $PtO_x/WO_3$ | — | 1.0 | 0.5 | — |
| 5 | $CrO_x$/Pt/$SrTiO_3$:Rh | $PtO_x/WO_3$ | $[Co(+)]^{3+}$ | 3.8 | 1.8 | 0 : 10 |
| 6 | $CrO_x$/Pt/$SrTiO_3$:Rh | $PtO_x/WO_3$ | $[Co(-)]^-$ | 1.2 | 2.3 | 10 : 0 |

[a] Standard conditions: $CrO_x$/Pt/$SrTiO_3$:Rh (70 mg) and $PtO_x/WO_3$ (70 mg) in an aqueous solution (pH 3.5, 70 mL) containing an electron mediator (0.3 mM) under visible-light irradiation ($\lambda = 430$ nm). [b] N.D. = not detected.

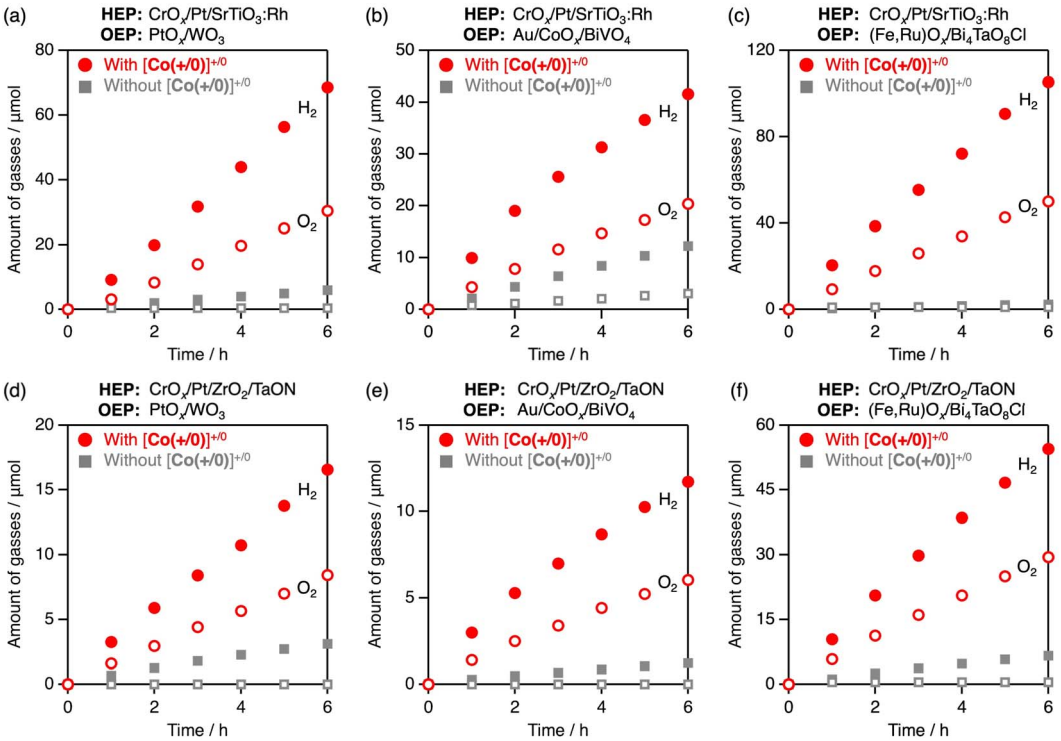


Fig. 8 Time courses of $H_2$ and $O_2$ evolution through Z-scheme water splitting in an aqueous solution (pH 3.5, 70 mL) in the presence or absence of $[Co(+/0)]^+$ (0.3 mM) as an electron mediator using the combination of (a) $CrO_x$/Pt/$SrTiO_3$:Rh–$PtO_x/WO_3$, (b) $CrO_x$/Pt/$SrTiO_3$:Rh–Au/$CoO_x$/$BiVO_4$, (c) $CrO_x$/Pt/$SrTiO_3$:Rh–(Fe,Ru)$O_x$/$Bi_4TaO_8Cl$, (d) $CrO_x$/Pt/$ZrO_2$/TaON–$PtO_x/WO_3$, (e) $CrO_x$/Pt/$ZrO_2$/TaON–Au/$CoO_x$/$BiVO_4$, and (f) $CrO_x$/Pt/$ZrO_2$/TaON–(Fe,Ru)$O_x$/$Bi_4TaO_8Cl$ (each 70 mg) under visible light irradiation ($\lambda = 430$ nm).

existence of the $[Co(-)]^-$ species significantly drops the $H_2$ evolution activity (Table 1). In the $[Co(+/0)]^{+/0}$ system, the $Co^{III}$/$Co^{II}$ balance was partially improved to some extent ($Co^{II}$ : $Co^{III}$ = 1 : 9, see entry 1 in Table 2). This improvement arises from the charge-switchable nature of the mediator, which alleviates the trade-off between forward and backward electron transfer in both $H_2$- and $O_2$-evolving reactions, as discussed above.

The AQE of the overall water splitting was recorded to be 2.0% at 405 nm when using the $[Co(+/0)]^{+/0}$ mediator. Although the $O_2$ evolution activity of the $PtO_x/WO_3$ photocatalyst still has considerable room for improvement, this performance represents the highest level reported to date for Z-scheme systems based on $SrTiO_3$:Rh and $WO_3$ photocatalysts using conventional redox mediators (Table S1).[31] The $[Co(+/0)]^{+/0}$ mediator was also applicable to Z-scheme overall water splitting under various combinations of HEP ($SrTiO_3$:Rh, TaON) and OEP ($WO_3$, $BiVO_4$, $Bi_4TaO_8Cl$) (Fig. 8). Among these combinations, the use of $SrTiO_3$:Rh and $Bi_4TaO_8Cl$ resulted in the best water-splitting performance, with an AQE of 2.7% at 430 nm.

## Conclusions

This study demonstrates the strong impact of manipulating the electrostatic interactions between photocatalyst surfaces and electron mediators to enhance the efficiency of Z-scheme water splitting systems. The designed charge-switchable $[Co(bpc)_2]^{+/0}$ complex represented an effective redox mediator, outperforming conventional cationic and anionic mediators. By selectively suppressing backward electron transfer without hindering forward electron transfer, the $[Co(bpc)_2]^{+/0}$ mediator improves the

performance in both half-reactions and overall Z-scheme water splitting, with an apparent quantum efficiency of 2.7% for overall water splitting using $SrTiO_3$:Rh and $Bi_4TaO_8Cl$ photocatalysts (improved from 1.6%[12] using $Fe^{3+/2+}$). To date, in contrast to the rational engineering of photocatalyst materials itself, the selection of the redox mediator has largely relied on "invisible" empirical compatibility in specific combinations of photocatalyst materials. This work provides clear design guidelines for the selection of electron mediators from the perspective of resistance toward backward electron transfer. The design of metal complex mediators has room for tuning their important properties such as redox potentials to further push up the Z-scheme water splitting performance, contributing to the advancement of solar hydrogen production technologies.

# Experimental section

### General procedure

$^1$H NMR (400 MHz) spectra were recorded using a JEOL ECX400 spectrometer. Crystallographic data were collected at 143 K on a Rigaku Saturn 724+ with Varimax equipment using graphite monochromated Mo-K$\alpha$ radiation ($\lambda = 0.71073$ Å). Powder X-ray diffraction patterns were recorded on MiniFlex II (Rigaku, X-ray source: Cu K$\alpha$). UV-visible absorption spectra were recorded at room temperature using a Shimadzu U1800 spectrometer. UV-visible diffuse reflectance spectra were recorded at room temperature on a Shimadzu U2600i spectrometer equipped with an integrating sphere. Cyclic voltammetry measurements were conducted on a BAS model 600F electrochemical analyser with a glassy carbon working electrode ($\phi = 3$ mm) and platinum wire counter electrode. The reference electrode, made of a silver wire, was inserted into a small glass tube fitted with a porous Vycor frit at the tip and filled with an aqueous solution containing 3 M NaCl. Zeta potentials were measured using a zeta potential analyser (Zetasizer Nano ZS, Malvern Instruments) in an aqueous solution under dark conditions. The pH of the solution was adjusted using HCl and NaOH. Transmission electron microscopy (TEM) images were obtained using a JEOL JEM-2100F microscope.

The amount of adsorbed cobalt complex was determined as follows. A suspension of $CrO_x$/Pt/$SrTiO_3$:Rh (1.5 mg) was dispersed in a 10 mL aqueous solution (pH 3.5, adjusted with HCl) containing cobalt complexes (*ca.* 0.3 mM) and stirred for 5 h in dark under an Ar atmosphere. The amount of adsorbed cobalt complexes was determined by UV-vis absorption spectroscopy. A cobalt complex solution without $CrO_x$/Pt/$SrTiO_3$:Rh was used as the blank control. Since there were cases where the chemical species changed before and after the experiment ($Co^{II}$ → $Co^{III}$ species), we estimated the adsorption amount by fitting the absorption spectra using the molar extinction coefficient and Lambert–Beer law for each complex (eqn (1) and Fig. S4).

$$\text{Fitting} = \varepsilon(Co^{II})[Co^{II}] + \varepsilon(Co^{III})[Co^{III}] \quad (1)$$

where $\varepsilon$(A) and [A] are molar extinction coefficient and concentration of a species "A", respectively.

### Synthesis of redox mediator

$[Co^{II}(tpyCO_2Me)_2]Cl_2$ ($[\mathbf{Co(+)}]^{2+}$), $[Co^{III}(tpyCO_2Me)_2]Cl_3$ ($[\mathbf{Co(+)}]^{3+}$), $Na_2[Co(dipic)_2]$ ($[\mathbf{Co(-)}]^{2-}$), and $Na[Co(dipic)_2]$ ($[\mathbf{Co(-)}]^{-}$) were synthesised according to a previously reported procedure.[37,38] $K_6[SiVW_{11}O_{40}]\cdot 6H_2O$ and $K_5[SiVW_{11}O_{40}]\cdot 14H_2O$ were prepared according to previously reported methods.[31,39]

$[Co^{II}(bpc)_2]^0$ ($[\mathbf{Co(+/0)}]^0$) was synthesised as follows: a 50 mL flask was charged with [2,2′-bipyridine]-6-carboxylic acid (bpcH, 1.0 g, 5.0 mmol, BLD pharm, >97.0%) and MeOH (33 mL, Wako Pure Chemical Industries Ltd, >99.8%). To this solution, tetramethylammonium hydroxide in MeOH (2.2 mL, 5.0 mmol, Sigma-Aldrich, 25 wt%) was added, affording a pale-yellow solution. $CoCl_2\cdot 6H_2O$ (594 mg, 2.5 mmol, Kanto Chemical Co. Inc., >99.0%) was then added, and the reaction mixture was heated at 65 °C under an Ar atmosphere overnight. The mixture was subsequently cooled to room temperature, and the precipitate was collected by filtration and washed with a small amount of MeOH. The obtained crude solid was dissolved in MeOH (*ca.* 160 mL) in a 200 mL flask and heated until almost complete dissolution. The hot solution was filtered, and the filtrate was placed in a freezer to promote crystallisation. The resulting red crystals were collected *via* filtration, washed three times with cold MeOH, and dried under vacuum to obtain $[Co^{II}(bpc)_2]$ (855.6 mg, 65% yield). $^1$H NMR (400 MHz, $D_2O$, Fig. S9a): $\delta$ 98.68 (s, 2H), 95.57 (s, 2H), 94.74 (s, 2H), 77.42 (s, 2H), 39.86 (s 2H), 24.16 (s, 2H), 17.38 (s, 2H). Anal. Calcd. for $C_{22}H_{14}N_4O_4Co\cdot H_2O$: C, 55.59; H, 3.39; N, 11.79; found: C, 55.81; H, 3.19; N, 11.76.

$[Co^{III}(bpc)_2]^+$ ($[\mathbf{Co(+/0)}]^+$) was synthesised *via* chemical oxidation as follows: a 30 mL vial was charged with $[Co^{II}(bpc)_2]^0$ (400 mg, 0.8 mmol) and MeCN (16.8 mL, Wako Pure Chemical Industries Ltd, > 99.5%). To this solution, $NO^+BF_4^-$ (153.2 mg, 1.3 mmol, Sigma-Aldrich, >95.0%) was added, and the mixture was stirred at room temperature for more than 1 h. The solvent was removed under reduced pressure, and the residue was dissolved in a minimal amount of $H_2O$ (*ca.* 2 mL). A saturated aqueous solution of $KPF_6$ (Wako Pure Chemical Industries Ltd, >99.5%) was added to this solution, and the resulting mixture was filtered through a membrane filter and washed with a small amount of water. The residue was then treated with Amberlite IRA-900J ion-exchange resin (Cl form) at room temperature for more than 30 min in water. After removing the resin by filtration, the filtrate was evaporated under reduced pressure. The product was dried under vacuum to obtain $[Co^{III}(bpc)_2]^+$ as a possible salt form $[Co^{III}(bpc)_2]Cl_{0.85}(PF_6)_{0.15}$ (335.7 mg, 73% yield). $^1$H NMR (400 MHz, $D_2O$, Fig. S9b): $\delta$ 9.10 (d, 2H), 8.98 (t, 2H), 8.63 (dd, 4H), 8.26 (t, 2H), 7.43 (t, 2H), 7.30 (d, 2H). Anal. Calcd. for $C_{22}H_{14}N_4O_4CoCl_{0.85}(PF_6)_{0.15}\cdot 2H_2O$: C, 48.47; H, 3.33; N, 10.28; found: C, 48.39; H, 3.13; N, 10.32. A summary of X-ray diffraction structural analysis for the MeOH-recrystallised single-crystal and crystallographic data is shown in Fig. S10 and Table S2.

### Synthesis of semiconductor photocatalysts

$SrTiO_3$:Rh,[29] $ZrO_2$/TaON,[35] surface-modified $WO_3$,[13] $BiVO_4$,[40] and $Bi_4TaO_8Cl$[22] were prepared according to previously reported

procedures, and their synthesis was confirmed by XRD and UV-visible differential reflectance spectroscopy (Fig. S11).

$CrO_x$/Pt/$SrTiO_3$:Rh was synthesised as follows. $SrCO_3$ (1.72 g, 11.6 mmol, Wako Pure Chemical Industries Ltd, >99.99%), rutile-$TiO_2$ (0.859 g, 10.8 mmol, Wako Pure Chemical Industries Ltd, >99.9%), and $Rh_2O_3$ (13.79 mg, 0.05 mmol, Wako Pure Chemical Industries Ltd, >99.99%) were used as starting materials. These were mixed in a mortar with an Sr : Ti : Rh atomic ratio of 1.07 : 0.99 : 0.01. The mixture was then transferred to an alumina crucible and subjected to preliminary calcination at 773 K in air for 2 h. After regrinding in a mortar, the mixture was subjected to main calcination at 1273 K in air for 10 h.[29] Pt cocatalyst loading onto $SrTiO_3$:Rh was performed by a photodeposition method.[29] First, the synthesised $SrTiO_3$:Rh powder was dispersed in a 10 vol% aqueous methanol solution containing $H_2PtCl_6$ (Wako Pure Chemical Industries Ltd, >99.9%) as a Pt precursor (0.3 wt% as metal). This suspension was irradiated with visible light ($\lambda$ > 420 nm) for 3 h at room temperature under an Ar atmosphere to photodeposit Pt. A 300 W Xenon lamp with an L-42 cutoff filter was used for light irradiation. The cocatalyst-loaded photocatalysts were collected by filtration, washed with water, and dried at room temperature in air. In the same manner, a $CrO_x$ shell was coated onto Pt/$SrTiO_3$:Rh using $K_2CrO_4$ (Wako Pure Chemical Industries Ltd, >99.0%) as a Cr precursor (0.45 wt% as metal) according to a previously reported procedure.[41]

$CrO_x$/Pt/$ZrO_2$/TaON was synthesised as follows. Zirconia-modified tantalum oxynitride ($ZrO_2$/TaON) was synthesised through a nitridation method.[35] First, $Ta_2O_5$ (1.33 g, 3.0 mmol, Kojundo Chemical Laboratory Co., Ltd, >99.9%) and $ZrO(NO_3)_2 \cdot 2H_2O$ (0.16 g, 0.6 mmol, Kanto Chemical Co. Inc., >99.0%) were mixed with a small amount of MeOH. This mixture was then calcined in air at 1073 K for 2 h in an alumina crucible to obtain the $ZrO_2$/$Ta_2O_5$ composite. Subsequently, this composite was subjected to nitridation under an $NH_3$ gas flow (12 mL $min^{-1}$) at 1123 K for 15 h to convert it into $ZrO_2$/TaON. The Pt cocatalyst was loaded onto $ZrO_2$/TaON *via* an impregnation method.[35] The $ZrO_2$/TaON powder was then dispersed in an aqueous solution containing $H_2PtCl_6$ as the Pt precursor (1.0 wt% as metal). After impregnation, the sample was dried and calcined at 473 K for 1 h under a $H_2$ flow. A $CrO_x$ shell was coated onto Pt/$ZrO_2$/TaON by the photodeposition method using $K_2CrO_4$ as the Cr precursor (1.5 wt% as metal) following the same procedure as for Pt/$SrTiO_3$:Rh.

$PtO_x$/$WO_3$ was synthesised as follows. $WO_3$ powder (10 g, Kojundo Chemical Laboratory Co., Ltd, >99.99%) was used as the starting material. The $WO_3$ powder was first thermally treated in air at 973 K for 2 h to improve its crystallinity. The powder was then suspended in water (500 mL) by ultrasonication for 15 min, and fine particles that did not precipitate were removed by decantation. This separation process was repeated three times, and the resulting powder was filtered and air-dried to afford large $WO_3$ particles. The $WO_3$ powder (1.0 g) was impregnated with 0.63 mL of an aqueous solution containing 110 mM CsCl (Wako Pure Chemical Industries Ltd, >99.0%), and the pH was adjusted to 1 using HCl (Wako Pure Chemical Industries Ltd, 6 M). The mixture was dried and calcined at 773 K for 30 min in air. Subsequently, Cs-modified $WO_3$ was suspended and stirred for 15 min in an aqueous solution (50 mL) containing 50 mM $FeSO_4$ and 1 M $H_2SO_4$. After treatment, the suspension was decanted to separate the solid product and then dried in air.[13] Then, a $PtO_x$ cocatalyst was loaded onto the surface-modified $WO_3$ by an impregnation method. The Fe–H–Cs–$WO_3$ powder was dispersed in an aqueous solution of $H_2PtCl_6$ as the Pt precursor (0.5 wt% as metal). After impregnation, the sample was dried and calcined at 823 K for 30 min in air to afford $PtO_x$/$WO_3$.[31]

Au/$CoO_x$/$BiVO_4$ was synthesised as follows. $BiVO_4$ was synthesised *via* a hydrothermal process according to a previously reported procedure.[40] The starting materials, $NH_4VO_3$ (1.17 g, 10 mmol, Wako Pure Chemical Industries Ltd, >99.0%) and $Bi(NO_3)_3 \cdot 5H_2O$ (4.85 g, 10 mmol, Wako Pure Chemical Industries Ltd, >99.5%), were dissolved in a 2.0 M $HNO_3$ solution (Wako Pure Chemical Industries Ltd, 69%), whose pH value was then adjusted to be about 0.5 using an $NH_3$ solution (Wako Pure Chemical Industries Ltd, 28.0%). The mixed solution was strongly stirred until a light-yellow precipitate was observed. This precipitate was further aged for 2 h and then transferred to a Teflon-lined stainless-steel autoclave for 10 h of hydrothermal treatment at 473 K. Au and $CoO_x$ cocatalysts were loaded onto $BiVO_4$ *via* a photodeposition method.[42] First, $BiVO_4$ powder was dispersed in an aqueous solution containing $HAuCl_4$ (Wako Pure Chemical Industries Ltd, >99.0%) as a Au precursor (0.8 wt% as metal). This suspension was irradiated for 2 h at 283 K under an Ar atmosphere to photodeposit Au. Second, through filtration, washing, and drying, the as-obtained powder was dispersed in a sodium buffer solution (pH 6.0, 50 mM) containing $CoSO_4$ (Wako Pure Chemical Industries Ltd, >99.5%) as a Co precursor (0.1 wt% as metal). This suspension was irradiated for 1 h at 283 K under an Ar atmosphere to photodeposit $CoO_x$. A 300 W xenon lamp with full-spectral irradiation was used for light irradiation.

(Fe,Ru)$O_x$/$Bi_4TaO_8Cl$ was synthesized as follows. $Bi_4TaO_8Cl$ was synthesized *via* a flux method according to a previously reported procedure.[22] $Bi_2O_3$ (Wako Pure Chemical Industries Ltd, >99.9%), $Ta_2O_5$ (Wako Pure Chemical Industries Ltd, >99.9%), and BiOCl (Wako Pure Chemical Industries Ltd, >95.0%) were mixed at the stoichiometric molar ratio required for $Bi_4TaO_8Cl$. The mixture was combined with a eutectic mixture of NaCl (Wako Pure Chemical Industries Ltd, >99.5%) and CsCl (35 : 65) as a flux, at a solute concentration ($Bi_4TaO_8Cl$/($Bi_4TaO_8Cl$ + flux)) of 5 mol%. The mixture (25 g) was placed in an alumina crucible and heated to 1023 K at a rate of 20 K $h^{-1}$. The product was thoroughly washed with deionised water and collected *via* filtration. The obtained powder samples were then dried at room temperature. Co-loading of the (Fe,Ru)$O_x$ cocatalyst was performed by simultaneous impregnation using $FeCl_3$ (Wako Pure Chemical Industries Ltd, >99.0%) and $RuCl_3$ (Wako Pure Chemical Industries Ltd, 85 wt%) precursors (0.5 and 0.9 wt% for Fe and Ru, respectively, *i.e.*, 10 mol% each for $Bi_4TaO_8Cl$).[12] A proper amount of the photocatalyst powder was dispersed in an aqueous solution containing the defined molar quantities of $FeCl_3$ and $RuCl_3$, followed by solvent evaporation in a water bath and heating at 573 K for 1 h under an Ar flow (20 mL $min^{-1}$).

### Photocatalytic reactions

Photocatalytic reactions were carried out in a Pyrex glass reactor under an Ar flow (20 mL $min^{-1}$). For the half-reaction of photocatalysis, a HEP (10 mg) or an OEP (35 mg) was dispersed in an aqueous solution (70 mL) containing an electron donor or acceptor (0.3 mM). The pH of the solution was adjusted by adding HCl or NaOH. For Z-scheme water splitting, HEP (70 mg) and OEP (70 mg) were dispersed in an aqueous solution (70 mL, pH 3.5 adjusted with HCl) containing an electron mediator (0.3 mM). The reaction dispersion was irradiated with visible light ($\lambda$ = 430 nm; 195 mW $cm^{-2}$) using an LED lamp (CL-H1-430-9-1-B and CL-H1LCB02, Asahi Spectra Co.). The generated gases were detected using a thermal conductivity detector (TCD) gas chromatograph (GC 3210D, GL Sciences, thermal conductivity detector, column packing: 5 Å molecular sieves, and Ar carrier gas) connected to the reaction system.

The apparent quantum efficiency (AQE) for $H_2$ evolution or Z-scheme water splitting was measured using the same experimental setup with bandpass filters and estimated according to eqn (2).

$$\text{AQE} = n \times (\text{amount of evolved } H_2)/(\text{amount of incident photons}) \quad (2)$$

where, $n$ indicates the number of photons required to generate one molecule of each product, *i.e.*, 2 for the $H_2$-evolving half-reaction and 4 for Z-scheme water splitting.

## Author contributions

R. I. and A. N. designed the study, with advice from H. S., O. T., and R. A. All remaining experiments were performed by R. I. All authors discussed the results. R. I. and A. N. wrote the manuscript.

## Conflicts of interest

There are no conflicts to declare.

## Data availability

The data supporting this article have been included in the main text and the supplementary information (SI). Supplementary information: UV-vis absorption spectra, cyclic voltammograms, photocatalytic activities for $H_2$ evolution, zeta potential, $^1$H NMR spectra, powder XRD patterns, and UV-vis absorption spectra. See DOI: https://doi.org/10.1039/d5sc10049f.

CCDC 2528130 contains the supplementary crystallographic data for this paper.[43]

## Acknowledgements

This work was supported by a JSPS KAKENHI grant (JP24K01603) and Grant-in-Aid for Transformative Research Areas "Concerto Photocatalysis" (JP23H03830 and JP23H03832). R. I. acknowledges support from the JSPS Fellowship for Young Scientists (JP23KJ1351). The authors are grateful to Profs. Kazuhiko Semba and Takayuki Tanaka (Kyoto University) for their kind support for single-crystal X-ray crystal structural analysis. Our acknowledgement is extended to Prof. Takaaki Toriyama (Kyushu University) for his support with TEM analysis. We express our gratitude to Mr Harutaka Ninomiya (Kyoto University) for his assistance in the synthesis of polyoxometalates.

## References

1 A. Fujishima and K. Honda, *Nature*, 1972, **238**, 37–38.
2 R. Abe, *Bull. Chem. Soc. Jpn.*, 2011, **84**, 1000–1030.
3 A. Kudo and Y. Miseki, *Chem. Soc. Rev.*, 2009, **38**, 253–278.
4 F. E. Osterloh, *Chem. Soc. Rev.*, 2013, **42**, 2294–2320.
5 S. Chen, T. Takata and K. Domen, *Nat. Rev. Mater.*, 2017, **2**, 17050.
6 C. Chen, W. Ma and J. Zhao, *Chem. Soc. Rev.*, 2010, **39**, 4206–4219.
7 Q. Wang and K. Domen, *Chem. Rev.*, 2020, **120**, 919–985.
8 Y. Wang, H. Suzuki, J. Xie, O. Tomita, D. J. Martin, M. Higashi, D. Kong, R. Abe and J. Tang, *Chem. Rev.*, 2018, **118**, 5201–5241.
9 M. Shi, X. Wu, Y. Zhao, R. Li and C. Li, *J. Am. Chem. Soc.*, 2025, **147**, 3641–3649.
10 H. Matsuoka, T. Inoue, H. Suzuki, O. Tomita, S. Nozawa, A. Nakada and R. Abe, *Sol. RRL*, 2023, **7**, 2300431.
11 H. Kato, Y. Sasaki, A. Iwase and A. Kudo, *Bull. Chem. Soc. Jpn.*, 2007, **80**, 2457–2464.
12 A. Nakada, H. Suzuki, J. J. M. Vequizo, K. Ogawa, M. Higashi, A. Saeki, A. Yamakata, H. Kageyama and R. Abe, *ACS Appl. Mater. Interfaces*, 2019, **11**, 45606–45611.
13 Y. Miseki and K. Sayama, *Catal. Sci. Technol.*, 2019, **9**, 2019–2024.
14 R. Abe, K. Sayama, K. Domen and H. Arakawa, *Chem. Phys. Lett.*, 2001, **344**, 339–344.
15 H. Kato, M. Hori, R. Konta, Y. Shimodaira and A. Kudo, *Chem. Lett.*, 2004, **33**, 1348–1349.
16 Y. Miseki, S. Fujiyoshi, T. Gunji and K. Sayama, *J. Phys. Chem. C*, 2017, **121**, 9691–9697.
17 Y. Sasaki, H. Kato and A. Kudo, *J. Am. Chem. Soc.*, 2013, **135**, 5441–5449.
18 K. Tsuji, O. Tomita, M. Higashi and R. Abe, *ChemSusChem*, 2016, **9**, 2201–2208.
19 Y. Sasaki, H. Nemoto, K. Saito and A. Kudo, *J. Phys. Chem. C*, 2009, **113**, 17536–17542.
20 I. Krivokapic, M. Zerara, M. L. Daku, A. Vargas, C. Enachescu, C. Ambrus, P. Tregenna-Piggott, N. Amstutz, E. Krausz and A. Hauser, *Coord. Chem. Rev.*, 2007, **251**, 364–378.
21 J. Resasco, H. Zhang, N. Kornienko, N. Becknell, H. Lee, J. Guo, A. L. Briseno and P. Yang, *ACS Cent. Sci.*, 2016, **2**, 80–88.
22 R. Itagaki, A. Nakada, H. Suzuki, O. Tomita, H.-C. Chang and R. Abe, *J. Am. Chem. Soc.*, 2025, **147**, 15567–15577.
23 Z. Pan, J. J. M. Vequizo, H. Yoshida, J. Li, X. Zheng, C. Chu, Q. Wang, M. Cai, S. Sun, K. Katayama, A. Yamakata and K. Domen, *Angew. Chem., Int. Ed.*, 2025, **64**, e202414628.

24 W.-J. Chun, A. Ishikawa, H. Fujisawa, T. Takata, J. N. Kondo, M. Hara, M. Kawai, Y. Matsumoto and K. Domen, *J. Phys. Chem. B*, 2003, **107**, 1798–1803.
25 M. Anik, *Electrochim. Acta*, 2009, **54**, 3943–3951.
26 F. Ambrosio, J. Wiktor and A. Pasquarello, *ACS Energy Lett.*, 2018, **3**, 829–834.
27 J. M. Bolts and M. S. Wrighton, *J. Phys. Chem.*, 1976, **80**, 2641–2645.
28 H. Suzuki, Y. Okada, S. Kise, X. Sui, S. Nozawa, O. Tomita and R. Abe, *ACS Catal.*, 2025, **15**, 4870–4879.
29 Y. Sasaki, A. Iwase, H. Kato and A. Kudo, *J. Catal.*, 2008, **259**, 133–137.
30 R. Abe, K. Shinmei, N. Koumura, K. Hara and B. Ohtani, *J. Am. Chem. Soc.*, 2013, **135**, 16872–16884.
31 O. Tomita, H. Naito, A. Nakada, M. Higashi and R. Abe, *Sustainable Energy Fuels*, 2022, **6**, 664–673.
32 A. J. Bard, R. Parsons and J. Jordan, *Standard Potentials in Aqueous Solution*, New York, 1985.
33 T. M. Suzuki, S. Yoshino, K. Sekizawa, Y. Yamaguchi, A. Kudo and T. Morikawa, *Appl. Catal., B*, 2022, **316**, 121600.
34 R. Abe, K. Sayama and H. Sugihara, *J. Phys. Chem. B*, 2005, **109**, 16052–16061.
35 K. Maeda, M. Higashi, D. Lu, R. Abe and K. Domen, *J. Am. Chem. Soc.*, 2010, **132**, 5858–5868.
36 Y. Miseki and K. Sayama, *RSC Adv.*, 2014, **4**, 8308.
37 E. C. Constable, K. Harris, C. E. Housecroft, M. Neuburger and J. A. Zampese, *CrystEngComm*, 2010, **12**, 2949–2961.
38 M. K. Tse, H. Jiao, G. Anilkumar, B. Bitterlich, F. G. Gelalcha and M. Beller, *J. Organomet. Chem.*, 2006, **691**, 4419–4433.
39 H. Ninomiya, O. Tomita, H. Suzuki, A. Nakada and R. Abe, *ACS Mater. Lett.*, 2024, **6**, 2474–2478.
40 Y. Qi, J. Zhang, Y. Kong, Y. Zhao, S. Chen, D. Li, W. Liu, Y. Chen, T. Xie, J. Cui, C. Li, K. Domen and F. Zhang, *Nat. Commun.*, 2022, **13**, 484.
41 K. Maeda, K. Teramura, D. Lu, N. Saito, Y. Inoue and K. Domen, *Angew. Chem., Int. Ed.*, 2006, **45**, 7806–7809.
42 Y. Qi, Y. Zhao, Y. Gao, D. Li, Z. Li, F. Zhang and C. Li, *Joule*, 2018, **2**, 2393–2402.
43 CCDC 2528130: Experimental Crystal Structure Determination, 2026, DOI: 10.5517/ccdc.csd.cc2qvqlx.